https://doi.org/10.2352/ISSN.2470-1173.2017.2.VIPC-408

Self-Example-Based Edge Enhancement Algorithm for Around View Monitor Images

Dong Yoon Choi[a], Ji Hoon Choi[a], Jin Wook Choi[b], Byung Cheol Song*[a]
[a]Inha University, Department of Electronic Engineering, 100, Inha-ro, Nam-gu, Incheon, Republic of Korea
[b]Hyundai Motor Company, ADAS Recognition Development Team, 150, Hyundai Yeonguso-ro, Hwaseong-si, Republic of Korea

Abstract

In general, edges in the peripheral areas of around view monitor (AVM) wide-angle (WA) images tend to be blurred. This paper proposes a self-example-based edge enhancement algorithm to improve the definition of such edges. First, a low-resolution (LR) version of a blurred WA high-resolution (HR) image is produced via down-scaling. Next, a proper self-example for each non-overlapped patch in the HR image is found within the LR image in terms of self-similarity. Then, high frequency information is extracted from the found LR patch, and it is finally added to the input HR patch. Experimental results show that the proposed algorithm provides higher JNBM values than previous works with outstanding visual quality.

Introduction

AVM (around view monitor) system stitches together a bird-eye view of a moving car from overhead and shows a moving image on the car's display, along with parking lot lane markings, curbs, and adjacent cars. It normally consist of four to six fish-eye or wide-angle (WA) cameras mounted around the vehicle, for example, one at the front bumper, another at the rear bumper, and one under each side mirror. Once an AVM image is generated, the next step is to detect and recognize object(s) in the image.

On the other hand, a WA lens refers to a lens whose focal length is substantially smaller than the focal length of a normal lens for a given film plane. This type of lens allows more of the scene to be included in the photograph, which is useful in architectural, interior and landscape photography where the photographer may not be able to move farther from the scene to photograph it. However, the peripheral area of the WA image tends to be blurred due to optical characteristic of WA lens. This phenomenon makes it difficult to detect or recognize object(s) around image boundary.

This problem can be solved if we can enhance edges in the peripheral area of the WA image. A simple method for edge enhancement is filtering [1-5]. As a typical filtering approach, conventional unsharp masking-based algorithms [1, 2] extract high frequency (HF) components from an input image, and add them to the input image for further enhancement of HF components. Those algorithms adjust edge strength by adaptively controlling gains of HF components. Similarly, some edge enhancement algorithms produce detail layers by filtering the input image [4, 5]. For instance, a famous guided filtering [5] effectively extracts detail layer using a guide image to avoid shooting phenomenon. However, since the above-mentioned algorithms should extract HF components or details directly from the input image, they may not work if the input image already loses entire HF components from the first. Note that the outer region of WA-images is usually blurred. So, such conventional edge enhancement algorithms may be not useful for the WA images. The direct solution to remove blur phenomenon can be deblur methods [6,7,11]. Conventional deblur algorithms estimate blur kernel of an input image, and reconstruct the latent image by deconvoluting the input image with the estimated blur kernel [7]. However, they can suffer from ringing artifacts and over-shooting phenomenon due to inaccurate estimation of blur kernel(s). Also, they are not suitable for real-time processing due to their huge computational complexity.

This paper proposes a self-example-based edge enhancement algorithm to sharpen the blurred boundaries of WA-images for AVM. First, a LR version of a blurred WA HR image is produced via down-scaling. Next, a proper self-example for each non-overlapped patch in the HR image is found within the LR image in terms of self-similarity. Then, HF information is extracted from the found LR patch, and it is finally added to the input HR patch. Experimental results show that the proposed algorithm provides superior visual quality to the previous works without any artifacts. Also, the proposed algorithm has higher average just noticeable blur metric (JNBM) [10] by about 0.39 than conventional sharpness enhancement algorithms.

The Proposed Algorithm

We propose a self-example-based edge enhancement algorithm for removing blur phenomenon in the peripheral area of WA-image.

Figure 1. (a) Wide-angle image, (b) estimated blur kernel of the red box, (c) estimated blur kernel of the blue box

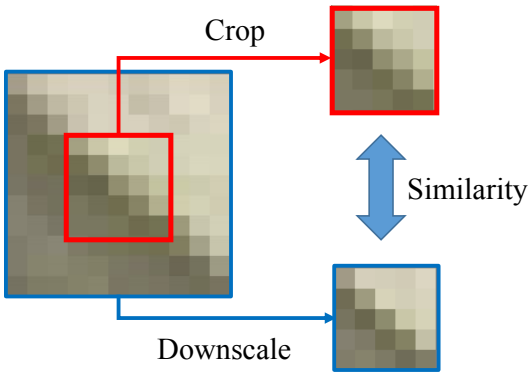

Figure 2. Basic concept of self-similarity

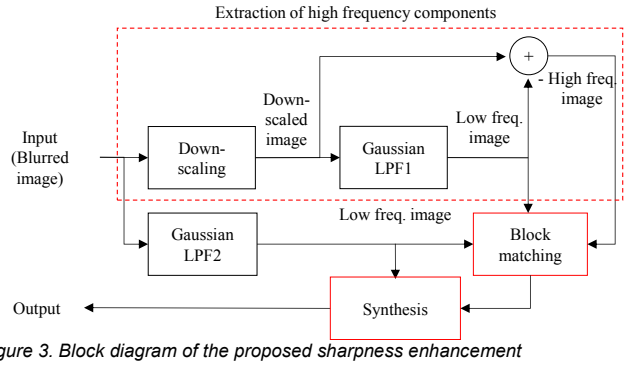

Figure 3. Block diagram of the proposed sharpness enhancement

Optical Characteristics of WA-images

Prior to description of the proposed algorithm, we need to analyze the optical characteristic of WA-images. Seeing images acquired by super-WA lens whose angle of view is greater than 180 degree, we can observe a sort of blur phenomenon in the boundaries of those images. Fig. 1 shows local blurness in a certain WA-image. For this experiment, we employed a state-of-the-art blur kernel estimation, i.e., Pan's algorithm [11]. We could observe that the blurness of the outer region is larger than that of the central area. According to our experiments, such a phenomenon is very general.

As mentioned previously, conventional filter-based edge enhancement algorithms cannot resolve this problem. Even deblur algorithms cannot be a practical solution because they rarely enhance edges without artefacts. Thus, we have to find an artefact-free edge enhancement algorithm for the outer region of WA-images.

The Proposed Algorithm

The key idea of the proposed algorithm is to apply HF components extracted from the down-scaled version of an input image for effective edge enhancement. Without loss of generality, down-scaled images tend to show sharper edges than their original resolution version. In other words, HF components which do not exist in the original images can be obtained from the down-scaled images if the same pattern exists on the different resolutions. In order to extract such HF information from the down-scaled images, we employ so-called self-similarity [8] (see Fig. 2). As shown in Fig. 2, an edge in an HR patch is very similar to that in its LR patch. This local feature is called self-similarity. This paper proposes an edge enhancement algorithm using self-similarity as in Fig. 3. The proposed algorithm consists of three steps: Extraction of HF components, self-similarity-based block matching between the input image and its down-scaled version, and HF synthesis.

Extraction of high frequency components

First, a linear operator $D_{\downarrow}$ for down-scaling is applied to an input image I, and a downscaled image I_D is produced as in Eq. (1).

$$I_D = D_{\downarrow} * I \tag{1}$$

where * indicates convolution. In this paper, Lanczos filter was used for down-scaling. Then, using Gaussian low-pass filter (LPF), i.e., LPF_1, I_D is decomposed into a low frequency (LF) image $I_{D,LF}$, and a HF image $I_{D,HF}$, respectively (see Eq. (2) and Eq. (3)).

$$I_{D,LF} = LPF_1 * I_D \tag{2}$$

$$I_{D,HF} = I_D - I_{D,LF} \tag{3}$$

Block matching

In this step, self-similarity-based block matching is performed between I and I_D. Here L_2-norm distance was used as a matching metric. The block or patch size for block matching was set to 5x5. In general, since frequency bands of I and I_D are different each other, block matching is applied to low-pass-filtered I and $I_{D,LF}$. A new Gaussian LPF for I, i.e. LPF_2, is employed so that low-pass-filtered I has similar frequency band to $I_{D,LF}$. So, low-pass-filtered I, i.e., I_{LF} is obtained by Eq. (4).

$$I_{LF} = LPF_2 * I \tag{4}$$

On the other hand, LPF_1 of Eq. (2) and LPF_2 of Eq. (4) have different standard deviations (σ). Via intensive experiments, we decided proper σ values providing minimum matching errors. In this paper, σ values for LPF_1 and LPF_2 were empirically set to 0.8 and 0.6, respectively.

The block matching between $I_{D,LF}$ and I_{LF} is performed on a block basis according to Eq. (5).

$$\arg\min_{\mathbf{p}'} \left\| I_{LF}(\mathbf{p}) - I_{D,LF}(\mathbf{p}') \right\|_2 \tag{5}$$

where $\mathbf{p}$ and $\mathbf{p}'$ are position vectors in I_{LF} and $I_{D,LF}$, respectively. And the search range to find $\mathbf{p}'$ was set to ± 2.

High frequency synthesis

If the best-match to a current patch $I_{LF}(\boldsymbol{p})$ within $I_{D,LF}$, i.e., $I_{D,LF}(\boldsymbol{p}')$ is found, its HF component $I_{D,HF}(\boldsymbol{p}')$ is derived via a conventional high pass filter. Finally, an edge-enhanced patch $O(\boldsymbol{p})$ is obtained by adding $I_{LF}(\boldsymbol{p})$ and $I_{D,HF}(\boldsymbol{p}')$ as in Eq. (6).

$$O(\boldsymbol{p}) = I_{LF}(\boldsymbol{p}) + I_{D,HF}(\boldsymbol{p}') \tag{6}$$

Iterative processing

Smaller down-scaling factor, sharper edges. On the contrary, smaller down-scaling factors make block matching difficult because similarly between two images having a large scale difference becomes lower. In order to solve such a trade-off problem, we employed two-stage processing as follows: In the first stage, an input image is down-scaled with a downscaling ratio of 2/3. Then, the down-scaled image is input to the basic edge enhancement system of Fig. 3. At this time, the down-scaling module in Fig. 3 is set to the scaling ratio of 1/2. As a result, block matching is performed between 1/2-downscaled and 2/3-down-scaled images. In the second stage, the output of the first stage becomes the down-scaled image in Fig. 3. So, block matching is performed between an original resolution and 2/3-down-scaled resolution images. Therefore, since the proposed multi-scale approach having a small scale difference between matching blocks increases accuracy of block matching, it can provide satisfactory visual quality.

Experimental Results

Evaluation in terms of Edge Enhancement

We compared the proposed algorithm with Polesel's algorithm [1], i.e., adaptive unsharp masking (AUM), Deng's algorithm [2], i.e., generalized unsharp masking (GUM), and two state-of-the-art deblur algorithms, i.e., Xu's algorithm [7], and Pan's algorithm [11]. Parameters for AUM are set as follows: $\tau_1 = 7$, $\tau_2 = 14$, $\alpha_{dh} = 2$, $\alpha_{dl} = 1.5$, $\mu = 0.1$, $\beta = 0.5$. Similarly, for GUM, $\Upsilon_{MAX} = 3$, $\Upsilon_{MIN} = 1$, and $\eta = 1$. On the other hand, we just employed the executable codes of Xu's and Pan's algorithms provided by the authors. All the parameters were set by default.

And we acquired various 720p test images by using a super-WA lens whose angle of view is 180 degree and used them as test images. Fig. 4 shows the thumbnails.

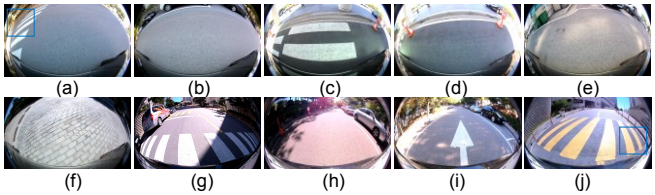

Figure 4. Thumbnails of test image set: (a) to (f) were named Test 1 to Test 10.

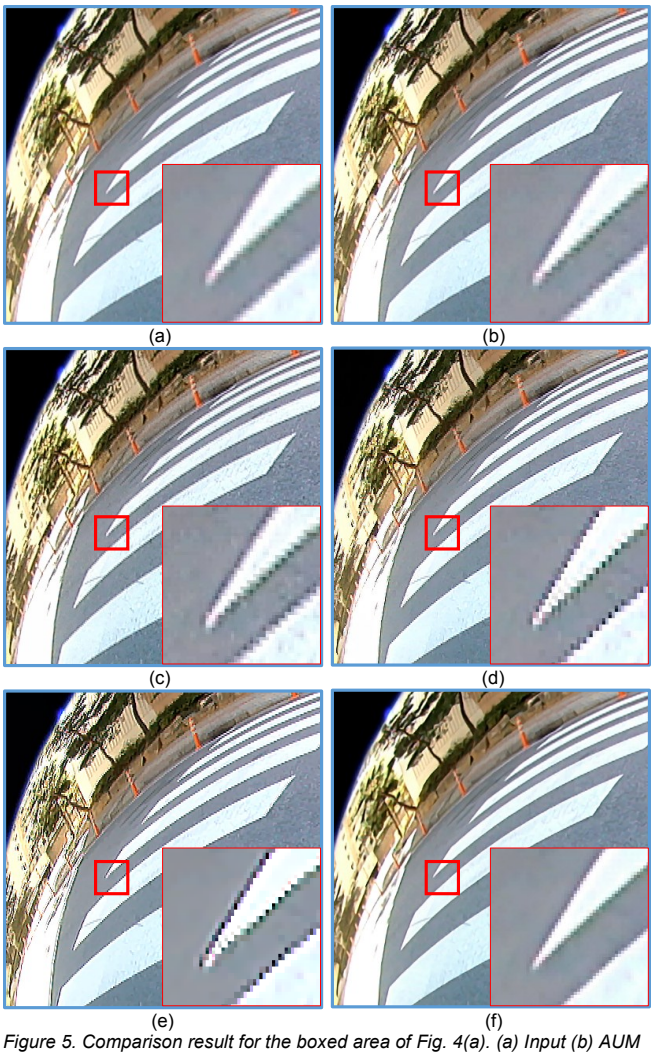

Figure 5. Comparison result for the boxed area of Fig. 4(a). (a) Input (b) AUM (c) GUM (d) Xu's (e) Pan's (f) proposed

Fig. 4(a)-(f) were shot at the left and Fig. 4(g)-(j) were shot at the rear of a vehicle, respectively. For example, Fig. 5 shows the result for a peripheral area (boxed region) of Fig. 4(a). Comparing lower-right enlarged images, we can observe that the proposed algorithm sharpens the blurred edges of the original image without any artifacts. However, GUM as well as AUM still show the blurred edges and suffer from jagging artefacts. Even though Xu's and Pan's algorithms enhance edge sharpness, they also suffer from staircase artefacts. Fig. 6 shows the result for a peripheral area (boxed region) of Fig. 4(j). Similarly to Fig. 5, we can see that the proposed algorithm enhances the blurred edges of the original image without any artifacts. On the contrary, unsharp masking-based methods seldom enhance the edges, and deconvolution-based methods such as Xu's and Pan's show unnatural edges. In sum, the previous approaches are not suitable for restoring the blurred outer region of WA images.

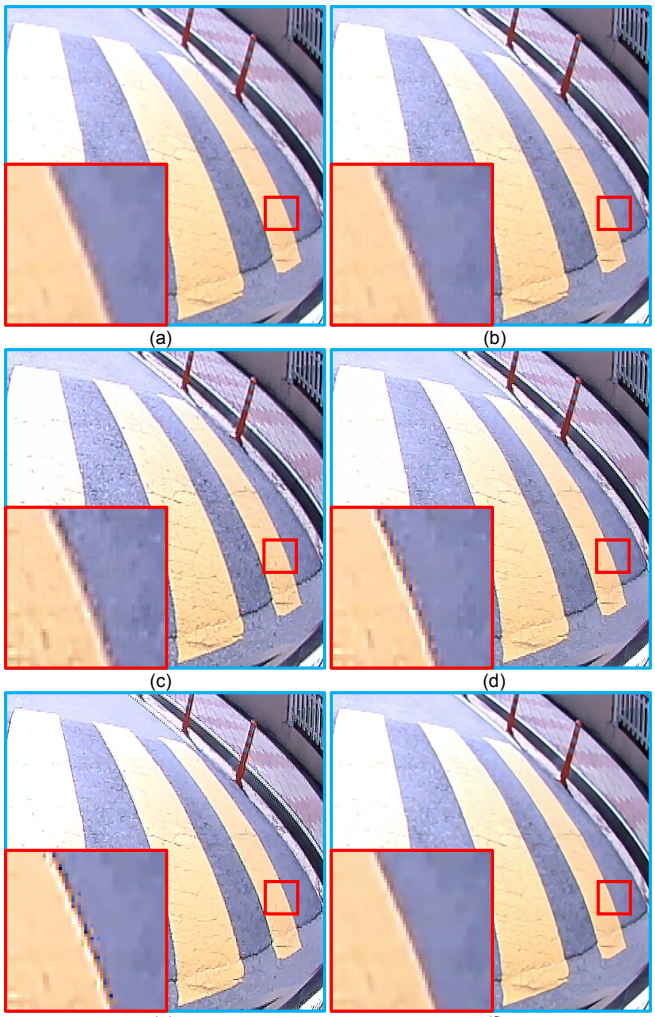

Figure 6. Comparison result for the boxed area of Fig. 4(a). (a) Input (b) AUM (c) GUM (d) Xu's (e) Pan's (f) proposed

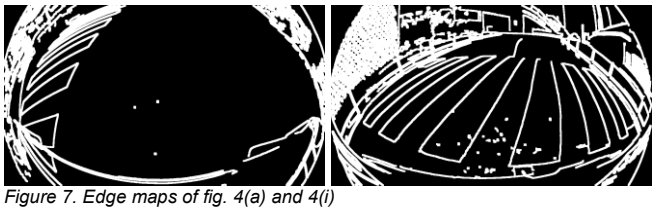

Figure 7. Edge maps of fig. 4(a) and 4(i)

For quantitative evaluation of the proposed algorithm, we employed an objective sharpness metric, i.e., JNBM. In order to fairly evaluate edge sharpness enhancement, we measured JNBM values only for edge pixels as in Fig. 7. For edge detection, Canny edge operator was used with dilation operation whose structure element is set to 7x7. Table I shows the JNBM results of each algorithm for all the test images. Note that higher JNBM values indicate better resolution.

Table I. Comparison in terms of JNBM

	Input	Polesel's	Deng's	Xu's	Pan's	Proposed
Test 1	9.9315	10.1924	10.4770	10.0160	10.9267	10.7281
Test 2	11.3339	11.7922	11.7169	12.1358	11.9895	11.8233
Test 3	8.5219	8.9489	8.7053	10.0459	9.6725	9.8933
Test 4	8.2571	8.6234	8.6067	9.5980	9.6650	9.2201
Test 5	8.2035	8.4896	8.8385	9.3395	9.5084	9.0778
Test 6	11.1667	12.3581	12.4890	14.4984	12.4465	12.5841
Test 7	10.3172	11.1344	10.9141	12.1786	10.9267	11.1457
Test 8	10.7116	11.2319	11.1214	11.9590	11.9895	11.2631
Test 9	10.0658	10.7580	10.7144	11.6470	12.4115	11.0449
Test 10	10.3905	11.1375	10.7554	11.8768	11.4199	11.4833
Ave.	9.8900	10.4666	10.4339	11.3295	11.0956	10.8264

The proposed algorithm provides higher JNBMs by 0.36 and 0.39 on average than AUM and GUM, respectively. Xu's and Pan's algorithms outperform the proposed algorithm in terms of JNBM, but this is due to excessive boosting of edges and staircase artefacts.

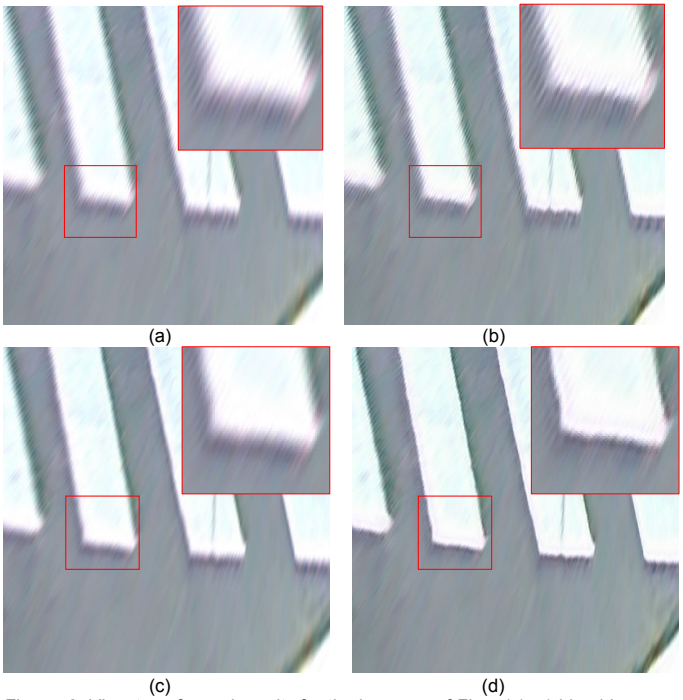

Figure. 8. View-transformed results for the box area of Fig. 4(a). a) bi-cubic w/o the proposed algorithm, (b) SR w/o the proposed algorithm, (c) bi-cubic w/ the proposed algorithm, (d) SR w/ the proposed algorithm.

Table II. Comparison of computational complexity [sec]

	AUM	GUM	Xu's	Pan's	Proposed
running time	0.096	0.234	9.213	2002.849	0.047

Integration with Up-scaling and View Transform

This subsection shows the integration of the proposed algorithm with up-scaling and view transform, that is a basic model of AVM. For two-times up-scaling, a super-resolution (SR) algorithm [9] was employed, and a conventional backward warping was used for WA-to-narrow angle (NA) view transform. The pixel-wise mapping between WA and NA images was empirically modelled and stored into a look-up-table (LUT). In the LUT-based backward warping, interpolation at noninteger pel was implemented by Lanczos filter. Fig. 8 shows the view-transformed results for the box area of Fig. 4(a). Comparing Fig. 8(b) and Fig. 8(d), we can find that edge enhancement by the proposed algorithm is outstanding.

Computational Complexity

Pan's algorithm was implemented in MATLAB, and the other algorithms were implemented in C language. All the algorithms were operated on i5-4570@3.20GHz with RAM of 16GB. We measured the average processing time for all the test images of Fig. 4. Note that Xu's and Pan's algorithms require huge complexity of about 9.2sec/frame and 2003sec/frame, respectively. Even though we consider Pan's algorithm is available in MATLAB code, its complexity is considerable. The proposed algorithm takes only 0.047sec/frame on average, which is the minimum among the comparative methods. This indicates that the proposed algorithm is suitable for real-time applications.

Concluding Remarks

This paper proposes a self-example-based edge enhancement algorithm to improve the definition of the blurred peripheral areas of wide-angle images. The proposed algorithm outperforms the previous edge enhancement algorithms subjectively as well as objectively. Especially, when the proposed algorithm is employed as the pre-processing for a conventional AVM, it can significantly improve visual quality of the AVM image. In addition, we showed that the proposed algorithm provides a high processing speed of 22Hz on general-purpose CPU environment.

Acknowledgment

This research was supported by Hyundai Motor Company (HMC, Korea), and supported by the Industrial Technology Innovation Program funded by the Ministry of Trade, industry & Energy (MI, Korea) [10052982, Development of multiangle front camera system for intersection AEB].

References

[1] A. Polesel, G. Ramponi and V. J. Mathews "Image enhancement via adaptive unsharp masking," *IEEE Transaction on Image Processing*, vol. 9, no. 3, pp. 505-510, 2000.

[2] G. Deng, "A Generalized unsharp masking algorithm," *IEEE Transaction on Image Processing*, vol. 20 no. 5, pp. 1249-1261, 2011.

[3] J. A. P. Tegenbosch, P. M. Hofman and M. K. Bosma, "Improving non-linear up-scaling by adaptive to the local edge orientation," *Proc. Visual Communication Image Processing*, vol. 5308, 2004.

[4] B. Zhang, J. P. Allebach, "Adaptive bilateral filter for sharpness enhancement and noise removal," *IEEE Transaction on Image Processing*, vol. 17, no. 5, pp. 664-678, 2008.

[5] K. He, J. Sun and X. Tang, "Guided image filtering," *IEEE Transactions on Pattern Analysis and Machine Intelligence*, vol. 35, no. 6, pp. 1397-1407, 2013.

[6] Krishnan and R. Fergus, "Fast image deconvolution using hyper-Laplacian priors," *Advances in Neural Information Processing Systems*, pp. 1033–1041, 2009.

[7] L. Xu , S. Zheng and J. Jia, "Unnatural L0 sparse representation for natural image deblurring," *Proc. IEEE Conference on Computer Vision and Pattern Recognition*, pp.1107-11142, 2013.

[8] G. Freedman and R. Fattal, "Image and video upscailng from local self-examples," *ACM Trans. on Graphics*, vol. 30, no. 2, Apr. 2011.

[9] D. Y. Choi and B. C. Song, "Fast super-resolution algorithm using ELBP classifier," *Proc. IEEE Visual Communications and Image Processing*, Dec. 2015.

[10] R. Ferzli and L. J. Karam, "A no-reference objective image sharpness metric based on the notion of just noticeable blur (JNB)," *IEEE Transaction on Image Processing*, pp. 717-728, 2009.

[11] J. Pan, D. Sun, H. Pfister and R. Ferzli and M. H. Yang, "Blind Image Deblurring Using Dark Channel Prior," *IEEE Computer Vision and Pattern Recognition*, pp. 1628-1636, 2016.

Author Biography

Dong Yoon Choi *received his B.S., M.S. degree in electronic engineering from Inha University, Incheon, Korea in 2014 and 2016. Currently, he is pursuing a Ph.D. degree in electronic engineering from Inha University. His research interests include image processing, super-resolution and deep-learning*

Ji-Hoon Choi *received his B.S. degree in electronic engineering from Inha University, Incheon, Korea in 2015. Currently, he is pursuing a M.S. degree in electronic engineering from Inha University. His research interests include image processing and super-resolution*

Jinwook Choi *received the B.S. and Ph.D. degrees from the School of Electrical and Electronic Engineering, Yonsei University, Seoul,Korea, in 2008 and 2014, respectively. He is currently a Senior Research Engineer with the ADAS Development Team of Automotive Research and Development Division, Hyundai Motor Company, Korea. His research interests include 2D/3D image and video processing, computer vision, hybrid sensor systems, and intelligent vehicle systems.*

Byung Cheol Song *received the B.S., M.S., and Ph.D. degrees in electrical engineering from the Korea Advanced Institute of Science and Technology (KAIST), Daejeon, Korea, in 1994, 1996, and 2001, respectively. From 2001 to 2008, he was a senior engineer at Digital Media R&D Center, Samsung Electronics Co., Ltd., Suwon, Korea. In March 2008, he joined the Department of Electronic Engineering, Inha University, Incheon, Korea, and currently is an associate professor. His research interests are in the general areas of image processing and computer vision.*